ACS APPLIED MATERIALS & INTERFACES

Research Article

Cite This: ACS Appl. Mater. Interfaces 2019, 11, 32046−32051

www.acsami.org

Artificial Solid-Electrolyte Interface Facilitating Dendrite-Free Zinc Metal Anodes via Nanowetting Effect

Mingqiang Liu,[‡] Luyi Yang,[‡] Hao Liu,[‡] Anna Amine, Qinghe Zhao, Yongli Song, Jinlong Yang, Ke Wang, and Feng Pan*

School of Advanced Materials, Peking University Shenzhen Graduate School, Shenzhen 518055, China

Supporting Information

ABSTRACT: The formation of dendrites on a zinc (Zn) metal anode has limited its practical applications on aqueous batteries. Herein, an artificial composite protective layer consisting of nanosized metal−organic frameworks (MOFs) to improve the poor wetting effect of aqueous electrolytes on the Zn anode is proposed to reconstruct the Zn/electrolyte interface. In this layer, hydrophilic MOF nanoparticles serve as interconnecting electrolyte reservoirs enabling nanolevel wetting effect as well as regulating an electrolyte flux on Zn anode. This zincophilic interface exhibits significantly reduced charge-transfer resistance. As a result, stable and dendrite-free Zn plating/stripping cycling performance is achieved for over 500 cycles. In addition, especially at higher C-rates, the coating layer significantly reduces the overpotentials in a Zn/MnO_2 aqueous battery during cycling. The proposed principle and method in this work demonstrate an effective way to reconstruct a stable interface on metal anodes (e.g., Zn) where a conventional solid-electrolyte interface (SEI) cannot be formed.

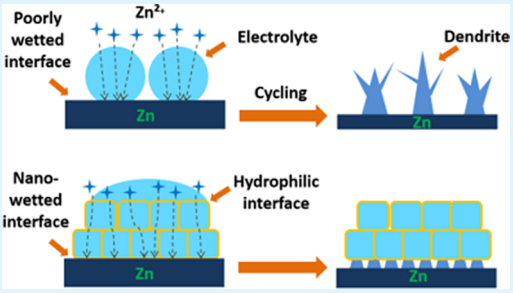

KEYWORDS: *zinc metal anode, zinc dendrite, artificial SEI, aqueous battery, nanowetting*

INTRODUCTION

Nowadays, research on inexpensive energy storage devices with excellent performance and a longer cycling life is becoming increasingly more important.[1] Compared with rechargeable batteries using organic electrolytes such as Li-ion batteries, water-based secondary batteries have drawn wide attention due to their low costs, safety, and environmental friendliness, which makes them suitable for mass production.[2] As an outstanding representative of water-based batteries, zinc (Zn) batteries, based on metallic Zn anodes, have many advantages such as abundant natural reserves, inexpensive price, high hydrogen evolution overpotential, high specific energy, high energy density, etc. Compared with lead−acid and nickel−cadmium batteries, zinc-based batteries are nontoxic and noncorrosive.[3,4] Zinc metal is still a widely used anode material in many Zn-based battery systems.[5−9] Among battery systems, Zn/MnO_2 batteries with neutral aqueous electrolytes demonstrate high energy density and cycling stability making them highly desirable for large-scale energy storage.[9,10] However, one main limiting factor for Zn batteries is the poor electrochemical reversibility of Zn in aqueous electrolytes.[11] Similar with Li anodes, owing to the uneven Zn deposition on the "hostless" negative electrode, the formation of dendritic metallic Zn metals could eventually penetrate the separator and cause a short circuit of the battery.[12−14] One possible solution is to replace the cycled Zn anode with fresh one,[15] which is not practical for large-scale energy grids. Methods such as electrolyte modification[3,16−18] and structured anodes[19−26] have been applied to improve the cycling stability of the Zn anode. Nevertheless, Zn electrodes with a high specific area suffer from low energy densities and more severe hydrogen evolution.[27] In addition, a backside charge/discharge reaction configuration of Zn anodes is designed to improve the longevity of metal-based batteries without short circuit.[28]

Unlike alkali metal anodes (e.g., Li and Na), solid-electrolyte interfaces (SEIs) cannot be formed between a Zn metal anode and an aqueous electrolyte. Consequently, the poorly wetted Zn anode by aqueous electrolytes could lead to high plating/stripping polarization; therefore, one promising strategy is to reconstruct an artificial SEI layer for the Zn anode to achieve a well-contacted interface. Herein, a thin protective coating layer that consists of poly(vinylidene fluoride) (PVDF) and an electrochemically inert microporous metal−organic framework (MOF) is applied on a Zn electrode by a simple method. Compared with the bare Zn metal anode, which exhibits poor wettability by aqueous electrolytes, the microporous structure of the MOF enables a nanolevel wetting effect with Zn and creates a zincophilic interface with significantly reduced interfacial charge-transfer resistance. The nanowetting effect facilitates an electrolyte flux on the Zn anode to maximize the interface contact between the solid and liquid resulting in a uniform Zn plating process at a current density of 3 mA cm^{-2} for over 500 cycles. Furthermore, Zn/MnO_2 aqueous batteries are also assembled and tested. It is found that compared to

Received: July 2, 2019
Accepted: August 13, 2019
Published: August 13, 2019

Downloaded via UNIV TOWN OF SHENZHEN on March 11, 2026 at 06:40:48 (UTC).
See https://pubs.acs.org/sharingguidelines for options on how to legitimately share published articles.

© 2019 American Chemical Society

DOI: 10.1021/acsami.9b11243
ACS Appl. Mater. Interfaces 2019, 11, 32046−32051

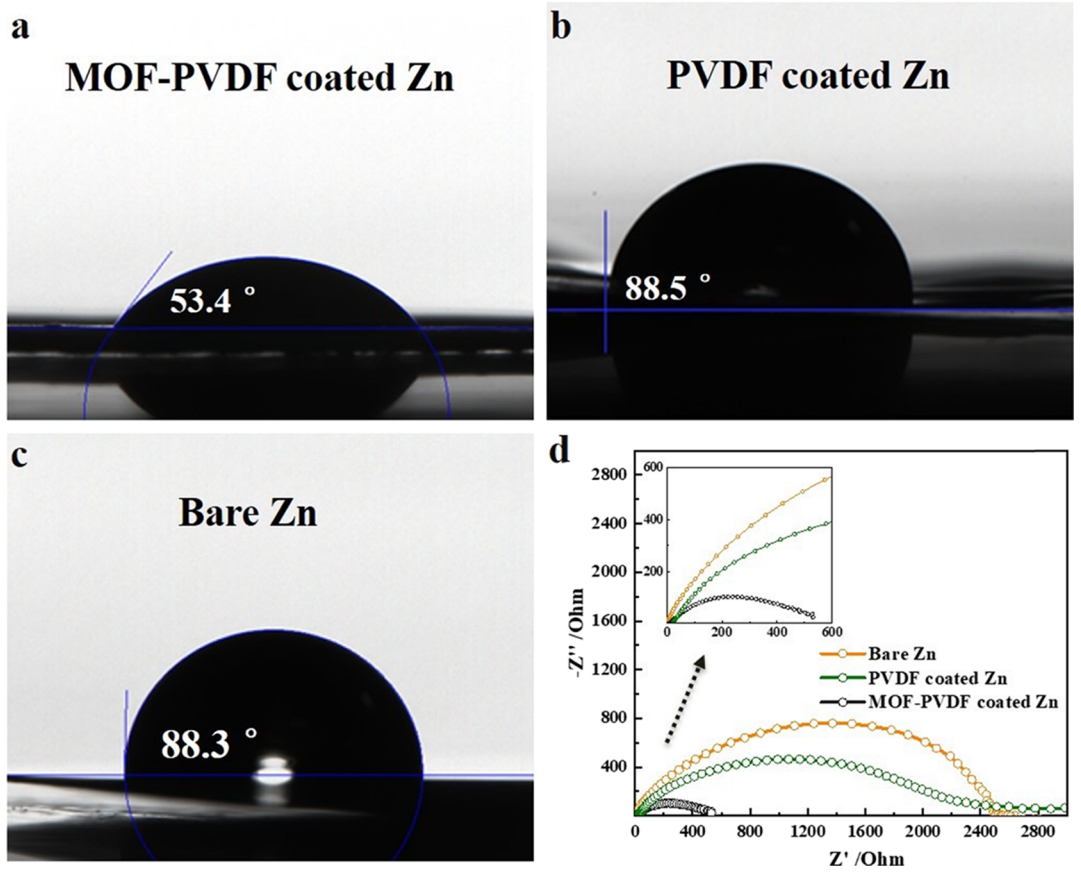

Figure 1. (a)−(c) Images of contact angles between the electrolyte and different anodes. (d) Electrochemical impedance spectra of Zn-symmetric cells with different anodes.

bare Zn, the coated Zn anode exhibits a significantly improved rate performance.

RESULTS AND DISCUSSIONS

Figure S1a shows the SEM image of as-prepared UIO-66 (Universistetet I Oslo-66) MOFs with an average particle size of 100 nm. The crystal information of the MOF particles is examined by X-ray diffraction (XRD). As shown in Figure S1b, all peaks are consistent with previously reported crystal structures.[29] Furthermore, according to the N_2 adsorption/desorption, results in the BET specific area and BJH pore volume of the MOF particles, presented in Figure S1c and Figure S1d, are measured to be 1276 $m^2\ g^{-1}$ and 0.64 $cm^3\ g^{-1}$, respectively. The pore size distribution also suggests the microporous structures of MOF particles. From the cross-section image of MOF−PVDF-coated Zn (shown in Figure S2), it can be observed that a dense layer of MOF−PVDF with an average thickness of 8 μm is coated in the Zn foil.

The wetting abilities of an aqueous electrolyte (3 M $ZnSO_4$ + 0.1 M $MnSO_4$) on different electrodes are compared in Figure 1a−c. It can be observed that the wetting angle of the electrolyte on PVDF-coated Zn (88.5°) is even slightly higher than that of bare Zn (88.3°), indicating that, due to its hydrophobic nature, the PVDF coating layer cannot improve the interfacial property between Zn and the electrolyte. By contrast, the addition of MOFs facilitates a hydrophilic interface by significantly lowering the wetting angle to 53.4°, which can be attributed to the hydrophilic surface and good water absorption capability of UIO-66 MOFs.[30] Since MOF

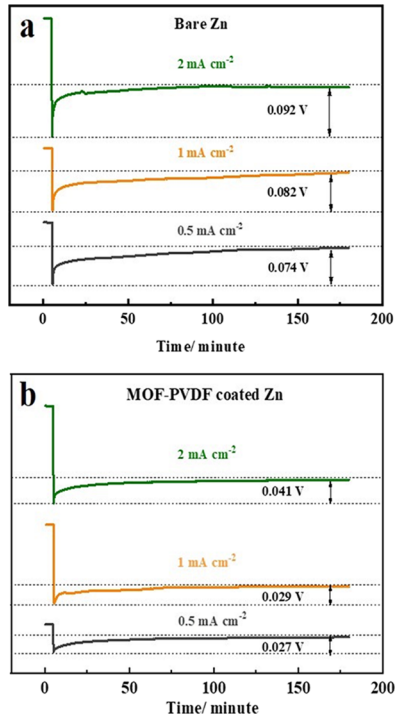

Figure 2. Voltage curves of Zn plating on (a) bare Zn and (b) coated Zn at various current densities.

particles are ideal carriers for the aqueous electrolyte, it is equally important to investigate the contact between Zn and

DOI: 10.1021/acsami.9b11243
ACS Appl. Mater. Interfaces 2019, 11, 32046−32051

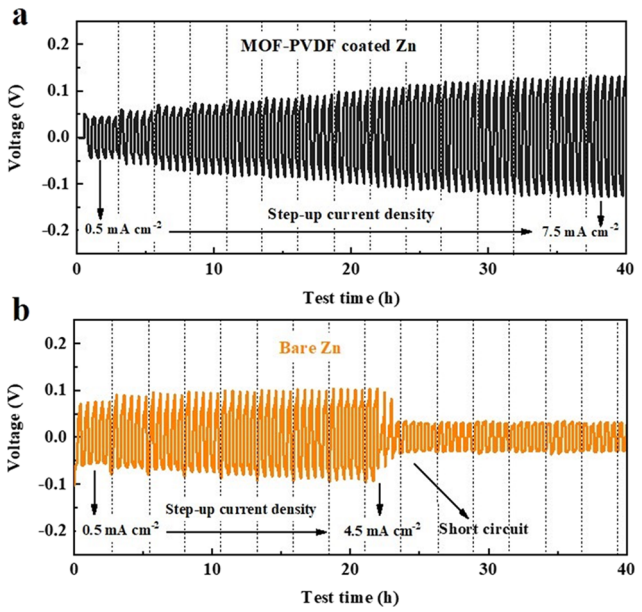

Figure 3. Voltage profiles of different Zn-symmetric cells using (a) coated Zn and (b) bare Zn during Zn plating/stripping using step-up current densities.

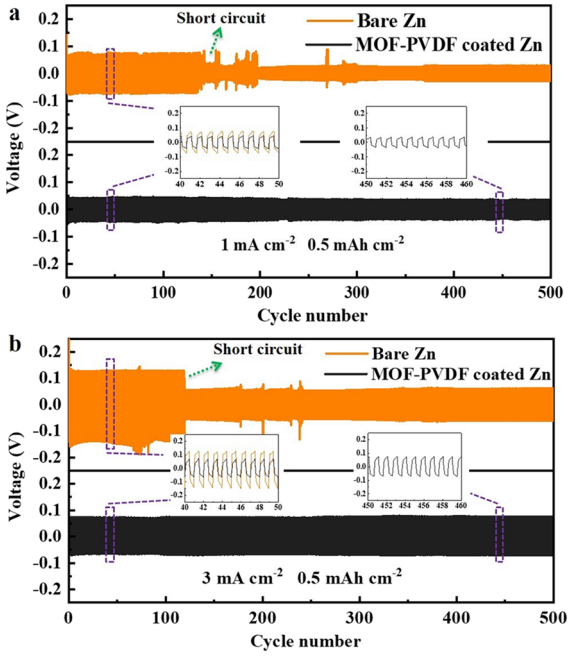

Figure 4. Voltage profiles of galvanostatic Zn plating/stripping for different Zn electrodes at (a) 1 mA cm^{-2} and (b) 3 mA cm^{-2}.

MOF particles, which are impregnated with an aqueous electrolyte. To explore this issue, first, electrochemical impedance spectroscopy (EIS) was carried out for Zn-symmetric cells using different anodes. As shown in Figure 1d, compared with bare Zn, the interfacial charge-transfer impedance (R_{ct}, represented by the semicircles in the Nyquist plot) between the electrolyte and Zn anode is significantly reduced from 2500 to 530 Ω in the presence of the MOF–PVDF coating layer. This indicates a greatly improved interfacial contact. To eliminate the effect of zinc oxide, Zn plating/stripping was carried out for 10 cycles. As shown in Figure S3, the cell coated with Zn still exhibits lower interfacial

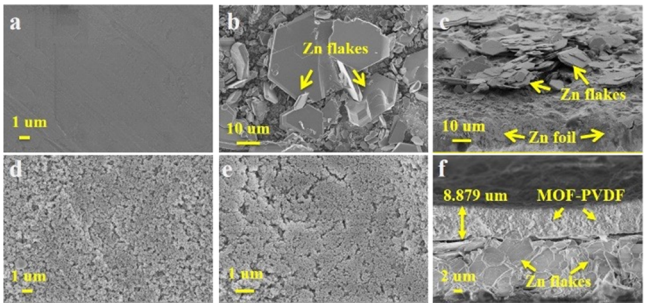

Figure 5. SEM images of bare Zn foil (a) before cycling and (b, c) after cycling and MOF-coated Zn foil (d) before cycling and (e, f) after cycling.

Scheme 1. Proposed Zn Plating Mechanisms on Bare Zn and MOF–PVDF-Coated Zn

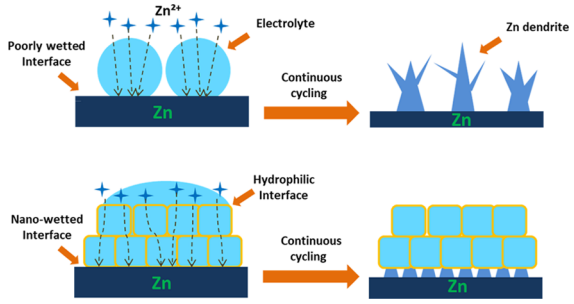

impedances. These results have shown that after impregnated with a liquid electrolyte, the coating layer exhibits excellent zincophilic features, which can be attributed to the nano-wetting effect of MOF particles.[31] Then, each MOF nanoparticle is closely contacted with Zn and served as a nanosized electrolyte reservoir. Consequently, this fully wetted solid–liquid interface exhibits a much lower charge-transfer resistance. The densely packed MOF particles also allow fast ion transport between wetted particle surfaces.

Similar to a lithium-metal deposition process,[32] voltage profiles of galvanostatic Zn plating processes on different electrodes can be used to evaluate the nucleation energy of Zn deposition. As shown in Figure 2, the Zn nucleation overpotentials on bare Zn are measured to be 92, 82, and 74 mV at current densities of 0.5, 1, and 2 mA cm^{-2}, respectively. In comparison, under the same current densities, the coating layer has reduced the nucleation overpotentials to 41, 29, and 29 mV, respectively. This result is in positive agreement with the cyclic voltameter results presented in Figure S4 where reduced overpotentials were obtained for both Zn deposition and stripping processes. As a result, the reduced nucleation overpotentials indicate lower nucleation energies as well as zincophilic interfaces facilitated by the MOF–PVDF coating. Ti/Zn cells were also fabricated to measure the Coulombic efficiency. It can be seen from Figure S5 that the coated Zn shows higher Coulombic efficiency compared with the bare Zn, indicating less severe side reactions (e.g., hydrogen evolution) during Zn plating/stripping on Ti current collectors.

Zn-symmetric cells were assembled to compare the Zn plating/stripping performances of different Zn electrodes. As shown in Figure 3, the current density increased to 7.5 mA cm^{-2}, and the voltage profiles MOF–PVDF-coated Zn remained very stable. The cell using bare Zn electrodes were

DOI: 10.1021/acsami.9b11243
ACS Appl. Mater. Interfaces 2019, 11, 32046–32051

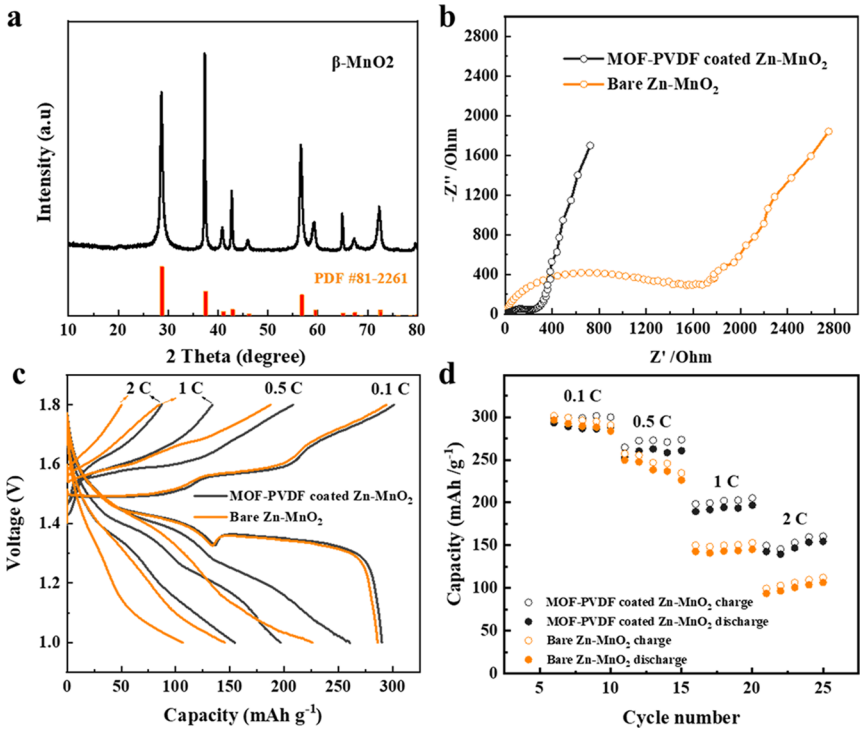

Figure 6. (a) XRD patterns of prepared MnO_2 cathode material, (b) electrochemical impedance spectra of Zn/MnO_2 cells using different anodes, and (c) voltage profiles and (d) rate performances of Zn/MnO_2 cells using different anodes under different C-rates.

short-circuited (as evidenced by the impedance spectra shown in Figure S6) due to the growth of Zn dendrites as the current density reached 4.5 mA cm^{-2}. This result indicates that the MOF−PVDF-coated Zn could withstand higher Zn plating/stripping current density without short circuit. For comparison, symmetric cells using PVDF-coated Zn electrodes are also tested. As shown in Figure S7, the voltage curve spiked when the current density increased to 1.5 mA cm^{-2}, indicating a large charge-transfer resistance.

Furthermore, the long-term cycling performances of Zn plating/stripping of different anodes are presented in Figure 4. The MOF−PVDF-coated Zn electrodes enable stable cycling for 500 cycles at the current densities of 1 and 3 mA cm^{-2}, whereas the cells with bare Zn electrodes, under the same testing condition, short-circuited after around 150 and 125 cycles. The improved cycling performances can be attributed to more uniform Zn plating/stripping behaviors in the presence of the coating layer; therefore, it can be clearly observed in the insets that the overpotentials of Zn plating/stripping on the MOF−PVDF-coated electrode is also significantly reduced compared to those on bare Zn. This further indicates reduced interfacial charge-transfer resistance enabled by the nanowetted interface. As shown in Figure S8, under a larger areal plating/stripping capacity of 3 mAh cm^{-2}, the coated Zn exhibits stable cycling for 100 h, whereas the bare Zn is short-circuited after 25 h.

To better understand the details of Zn plating/stripping electrochemistry, the postcycling SEM images of different Zn electrodes are presented in Figure 5. From Figure 5a−c, it can be clearly observed that after 200 cycles at a current density of 1 mA cm^{-2}, significant morphology changes can be observed: not only micron-sized Zn flakes are to be formed but severe Zn pulverization can also be observed in Figure 5c. By contrast, as shown in Figure 5d,e, the morphology of the PVDF−MOF-coated electrode remains almost unchanged after cycling. From the cross section in Figure 5f, it can be observed that the MOF−PVDF coating layer remains perfectly intact. Compared with Figure 5c, a much denser Zn layer is formed under the MOF−PVDF layer in Figure 5f. The proposed schematic illustration of different Zn plating mechanisms is presented in Scheme 1. The poor interfacial wetting of the electrolyte on the bare Zn anode leads to localized current flow, which further causes dendrite formation, but, on the other hand, the MOF particles impregnated with electrolyte enables well-contacted interfaces and regulates uniform Zn plating, hence the dendrite formation that can be suppressed.

To investigate the impact of this coating strategy on practical uses, Zn|MnO_2 batteries using bare Zn and the coated Zn anode are assembled and tested. The XRD pattern of the cathode material is presented in Figure 6a, which can be indexed to β-MnO_2. In addition, the SEM image of the prepared δ-MnO_2 (Figure S9) exhibits morphology of nanorods with a diameter of 50 nm. From Figure 6b, it can be observed that the cell using the MOF−PVDF-coated Zn anode exhibits much lower interfacial impedance than the cell using the bare Zn anode, which is in correlation with the results in Figure 2a. The cyclic voltammograms of both cells are compared in Figure S10: two cathodic peaks at 1.38 and 1.24 V are attributed to the 2 electron reduction from Mn^{4+} to Mn^{2+}, whereas two asymmetric anodic peaks at 1.58 and 1.62 V represent the reverse oxidation processes. Next, rate capability tests were performed for both cells, and the voltage curves of both cells are presented in Figure 6c where both discharging and charging curves exhibit two plateaus, which correspond to the 2 electron redox reactions. At a C-rate of 0.1 C, the cell using coated Zn exhibits a slightly lower overpotential compared with the cell using bare Zn due to the lower interfacial impedance. As the current increases, the

DOI: 10.1021/acsami.9b11243
ACS Appl. Mater. Interfaces 2019, 11, 32046−32051

difference in overpotentials becomes more evident. As a result, better rate performance is achieved by the cell using the coated Zn electrode (as shown in Figure 6d). In addition, the long-term cycling stability of both cells was also tested and compared in Figure S11. After 5 cycles, the cell with the coated Zn anode achieved higher capacity retention compared to the cell using bare Zn, which could be ascribed to the higher stability of the coated Zn anode.

CONCLUSIONS

To summarize, a thin protective layer consisting of MOFs and PVDF is applied on a Zn anode to pursue stable Zn anodes in aqueous electrolytes. It is found that instead of a poorly wetted interface between bare Zn and an aqueous electrolyte, a zincophilic interface with a lowered Zn plating nucleation overpotential is achieved by the MOF−PVDF coating layer, owing to the nanowetting effect of electrolyte-impregnated MOF nanoparticles. Results have shown that the coated Zn anode allows stable Zn plating/stripping at a current density of as high as 7.5 mA cm^{-2} without short circuit. In addition, a stable cycling performance is achieved by the coated Zn anode for over 500 cycles at 3 mA cm^{-2}. It is proposed that uniform Zn plating is enabled by the nanoscale interfacial contact as well as the regulated current flow on the Zn electrode, which further leads to a dendrite-free Zn anode. The performance of coated Zn is, also, evaluated in a Zn/MnO_2 aqueous battery. The results show that the coating significantly reduces the overpotential during cycling, especially at higher C-rates. Improved full-cell cycling stability is also exhibited by the coated Zn anode. The proposed principle and method in this work could offer useful guidance on future protection for metal anodes with dendrite issues.

ASSOCIATED CONTENT

Supporting Information

The Supporting Information is available free of charge on the ACS Publications website at DOI: 10.1021/acsami.9b11243.

Experimental methods, BET measurement, SEM images, and additional electrochemical test results (PDF)

AUTHOR INFORMATION

Corresponding Author

*E-mail: panfeng@pkusz.edu.cn.

ORCID

Luyi Yang: 0000-0002-5516-9829

Feng Pan: 0000-0002-8216-1339

Author Contributions

‡M.L., L.Y., and H.L. contributed equally. The manuscript was written through contributions of all authors. All authors have given approval to the final version of the manuscript.

Notes

The authors declare no competing financial interest.

ACKNOWLEDGMENTS

This research was financially supported by Soft Science Research Project of Guangdong Province (2017B030301013) and Shenzhen Science and Technology Research Grant (JCYJ20160226105838578 and ZDSYS201707281026184).

REFERENCES

(1) Liu, T.; Lin, L.; Bi, X.; Tian, L.; Yang, K.; Liu, J.; Li, M.; Chen, Z.; Lu, J.; Amine, K.; Xu, K.; Pan, F. In Situ Quantification of Interphasial Chemistry in Li-Ion Battery. *Nat. Nanotechnol.* **2019**, *14*, 50−56.

(2) Chang, Z.; Yang, Y.; Li, M.; Wang, X.; Wu, Y. Green Energy Storage Chemistries Based on Neutral Aqueous Electrolytes. *J. Mater. Chem. A* **2014**, *2*, 10739−10755.

(3) Zhang, N.; Cheng, F.; Liu, Y.; Zhao, Q.; Lei, K.; Chen, C.; Liu, X.; Chen, J. Cation-Deficient Spinel $ZnMn_2O_4$ Cathode in Zn-$(CF_3SO_3)_2$ Electrolyte for Rechargeable Aqueous Zn-Ion Battery. *J. Am. Chem. Soc.* **2016**, *138*, 12894−12901.

(4) Xu, C.; Li, B.; Du, H.; Kang, F. Energetic Zinc Ion Chemistry: The Rechargeable Zinc Ion Battery. *Angew. Chem., Int. Ed.* **2012**, *51*, 933−935.

(5) Parker, J. F.; Chervin, C. N.; Pala, I. R.; Machler, M.; Burz, M. F.; Long, J. W.; Rolison, D. R. Rechargeable Nickel-3D Zinc Batteries: An Energy-Dense, Safer Alternative to Lithium-Ion. *Science* **2017**, *356*, 415−418.

(6) Lee, J.-S.; Tai Kim, S.; Cao, R.; Choi, N.-S.; Liu, M.; Lee, K. T.; Cho, J. Metal−Air Batteries with High Energy Density: Li−Air versus Zn−Air. *Adv. Energy Mater.* **2011**, *1*, 34−50.

(7) Kundu, D.; Adams, B. D.; Duffort, V.; Vajargah, S. H.; Nazar, L. F. A High-Capacity and Long-Life Aqueous Rechargeable Zinc Battery Using a Metal Oxide Intercalation Cathode. *Nat. Energy* **2016**, *1*, 16119.

(8) Wang, X.; Wang, F.; Wang, L.; Li, M.; Wang, Y.; Chen, B.; Zhu, Y.; Fu, L.; Zha, L.; Zhang, L.; Wu, Y.; Huang, W. An Aqueous Rechargeable Zn//Co_3O_4 Battery with High Energy Density and Good Cycling Behavior. *Adv. Mater.* **2016**, *28*, 4904−4911.

(9) Pan, H.; Shao, Y.; Yan, P.; Cheng, Y.; Han, K. S.; Nie, Z.; Wang, C.; Yang, J.; Li, X.; Bhattacharya, P.; Mueller, K. T.; Liu, J. Reversible Aqueous Zinc/Manganese Oxide Energy Storage from Conversion Reactions. *Nat. Energy* **2016**, *1*, 16039.

(10) Beck, F.; Rüetschi, P. Rechargeable Batteries with Aqueous Electrolytes. *Electrochim. Acta* **2000**, *45*, 2467−2482.

(11) Dell, R. M. Batteries - Fifty Years of Materials Development. *Solid State Ionics* **2000**, *134*, 139−158.

(12) Matsushita, M.; Sano, M.; Hayakawa, Y.; Honjo, H.; Sawada, Y. Fractal Structures of Zinc Metal Leaves Grown by Electrodeposition. *Phys. Rev. Lett.* **1984**, *53*, 286−289.

(13) Hepel, T. Effect of Surface Diffusion in Electrodeposition of Fractal Structures. *J. Electrochem. Soc.* **1987**, *134*, 2685−2690.

(14) Yang, L.; Wang, Z.; Feng, Y.; Tan, R.; Zuo, Y.; Gao, R.; Zhao, Y.; Han, L.; Wang, Z.; Pan, F. Flexible Composite Solid Electrolyte Facilitating Highly Stable "Soft Contacting" Li−Electrolyte Interface for Solid State Lithium-Ion Batteries. *Adv. Energy Mater.* **2017**, *7*, 1701437.

(15) Fu, J.; Cano, Z. P.; Park, M. G.; Yu, A.; Fowler, M.; Chen, Z. Electrically Rechargeable Zinc-Air Batteries: Progress, Challenges, and Perspectives. *Adv. Mater.* **2017**, *29*, 1604685.

(16) Sun, K. E. K.; Hoang, T. K. A.; Doan, T. N. L.; Yu, Y.; Zhu, X.; Tian, Y.; Chen, P. Suppression of Dendrite Formation and Corrosion on Zinc Anode of Secondary Aqueous Batteries. *ACS Appl. Mater. Interfaces* **2017**, *9*, 9681−9687.

(17) Zhao, J.; Zhang, J.; Yang, W.; Chen, B.; Zhao, Z.; Qiu, H.; Dong, S.; Zhou, X.; Cui, G.; Chen, L. "Water-in-Deep Eutectic Solvent" Electrolytes Enable Zinc Metal Anodes for Rechargeable Aqueous Batteries. *Nano Energy* **2019**, *57*, 625−634.

(18) Wang, F.; Borodin, O.; Gao, T.; Fan, X.; Sun, W.; Han, F.; Faraone, A.; Dura, J. A.; Xu, K.; Wang, C. Highly Reversible Zinc Metal Anode for Aqueous Batteries. *Nat. Mater.* **2018**, *17*, 543−549.

(19) Lee, S.-H.; Yi, C.-W.; Kim, K. Characteristics and Electrochemical Performance of the TiO_2-Coated ZnO Anode for Ni - Zn Secondary Batteries. *J. Phys. Chem. C* **2011**, *115*, 2572−2577.

(20) Chamoun, M.; Hertzberg, B. J.; Gupta, T.; Davies, D.; Bhadra, S.; Van Tassell, B.; Erdonmez, C.; Steingart, D. A. Hyper-Dendritic Nanoporous Zinc Foam Anodes. *NPG Asia Mater.* **2015**, *7*, e178.

DOI: 10.1021/acsami.9b11243
ACS Appl. Mater. Interfaces 2019, 11, 32046−32051

(21) Caldeira, V.; Rouget, R.; Fourgeot, F.; Thiel, J.; Lacoste, F.; Dubau, L.; Chatenet, M. Controlling the Shape Change and Dendritic Growth in Zn Negative Electrodes for Application in Zn / Ni Batteries. *J. Power Sources* **2017**, *350*, 109−116.
(22) Shen, C.; Li, X.; Li, N.; Xie, K.; Wang, J.-g.; Liu, X.; Wei, B. Graphene-Boosted, High-Performance Aqueous Zn-Ion Battery. *ACS Appl. Mater. Interfaces* **2018**, *10*, 25446−25453.
(23) Wang, Z.; Huang, J.; Guo, Z.; Dong, X.; Liu, Y.; Wang, Y.; Xia, Y. A Metal-Organic Framework Host for Highly Reversible Dendrite-Free Zinc Metal Anodes. *Joule* **2019**, *3*, 1289−1300.
(24) Wu, Y.; Zhang, Y.; Ma, Y.; Howe, J. D.; Yang, H.; Chen, P.; Aluri, S.; Liu, N. Ion-Sieving Carbon Nanoshells for Deeply Rechargeable Zn-Based Aqueous Batteries. *Adv. Energy Mater.* **2018**, *8*, 1802470.
(25) Wu, T.-H.; Zhang, Y.; Althouse, Z. D.; Liu, N. Nanoscale Design of Zinc Anodes for High-Energy Aqueous Rechargeable Batteries. *Mater. Today Nano* **2019**, *6*, 100032.
(26) Zhang, Y.; Wu, Y.; Ding, H.; Yan, Y.; Zhou, Z.; Ding, Y.; Liu, N. Sealing ZnO Nanorods for Deeply Rechargeable High-Energy Aqueous Battery Anodes. *Nano Energy* **2018**, *53*, 666−674.
(27) Cheng, X.-B.; Zhang, R.; Zhao, C.-Z.; Zhang, Q. Toward Safe Lithium Metal Anode in Rechargeable Batteries: A Review. *Chem. Rev.* **2017**, *117*, 10403−10473.
(28) Higashi, S.; Lee, S. W.; Lee, J. S.; Takechi, K.; Cui, Y. Avoiding Short Circuits from Zinc Metal Dendrites in Anode by Backside-Plating Configuration. *Nat. Commun.* **2016**, *7*, 11801.
(29) Wang, S.; Morris, W.; Liu, Y.; McGuirk, C. M.; Zhou, Y.; Hupp, J. T.; Farha, O. K.; Mirkin, C. A. Surface-Specific Functionalization of Nanoscale Metal-Organic Frameworks. *Angew. Chem., Int. Ed.* **2015**, *54*, 14738−14742.
(30) Liu, X.; Demir, N. K.; Wu, Z.; Li, K. Highly Water-Stable Zirconium Metal-Organic Framework UiO-66 Membranes Supported on Alumina Hollow Fibers for Desalination. *J. Am. Chem. Soc.* **2015**, *137*, 6999−7002.
(31) Wang, K.; Yang, L.; Wang, Z.; Zhao, Y.; Wang, Z.; Han, L.; Song, Y.; Pan, F. Enhanced Lithium Dendrite Suppressing Capability Enabled by a Solid-like Electrolyte with Different-Sized Nanoparticles. *Chem. Commun.* **2018**, *54*, 13060−13063.
(32) Yan, K.; Lu, Z.; Lee, H.-W.; Xiong, F.; Hsu, P.-C.; Li, Y.; Zhao, J.; Chu, S.; Cui, Y. Selective Deposition and Stable Encapsulation of Lithium through Heterogeneous Seeded Growth. *Nat. Energy* **2016**, *1*, 16010.

DOI: 10.1021/acsami.9b11243
ACS Appl. Mater. Interfaces 2019, 11, 32046−32051